

Siegen University SI-96-12
October 1996

HADRONIC PHOTON INTERACTIONS AT HIGH ENERGIES ^a

F.W. Bopp

Universität Siegen, Fachbereich Physik, D-57068 Siegen, Germany

R. Engel

Institut für Theoretische Physik

Universität Leipzig, D-04109 Leipzig, Germany

and Universität Siegen, Fachbereich Physik, D-57068 Siegen, Germany

A. Rostovtsev

LPNHE Paris Université Paris VI, IN2P3-CNRS, France

and Institute of Theoretical and Experimental Physics Moscow, Russia

A simple phenomenological introduction to the physics of multi-pomeron exchange amplitudes in connection with the Abramovski-Gribov-Kancheli (AGK) cutting rules is given. The AGK cutting rules are applied to obtain qualitative and quantitative predictions on multiparticle production at high energies. On this basis, particle production in hadron-hadron scattering, photoproduction, and in particular the transition to deep-inelastic scattering is discussed.

1 Multi-pomeron exchange phenomenology

Assuming that high virtual masses are damped due to the dynamics of the the strong interaction, hadronic interactions can be described by Gribov's Reggeon field theory (RFT)^{1,2,3}. In RFT, hadronic scattering is characterized by the exchange of pomerons. The total amplitude can be written as the sum of n -pomeron exchange amplitudes $A^{(n)}(s, t)$. For each n -pomeron graph one can define a theoretical "total" cross section applying the optical theorem ($\sigma_{\text{tot}} = \Im m(A)$, implicitly $t = 0$ is taken)

$$\sigma^{(n)} = (-1)^{n+1} \Im m \left(A^{(n)} \right), \quad \sigma_{\text{tot}} = \sum_{n=1}^{\infty} (-1)^{n+1} \sigma^{(n)}. \quad (1)$$

Here, an alternating sign has been introduced by definition to keep all partial cross sections $\sigma^{(n)}$ positive.

To keep the arguments as simple as possible, we restrict the discussion to the graphs shown in Fig. 1, $\sigma^{(n)} \ll 4\sigma^{(2)} < \sigma^{(1)}$ with $n > 2$. Then, the

^aTalk presented by R. Engel at the XXVI Int. Symposium on Multiparticle Dynamics, Faro, Portugal, 1996

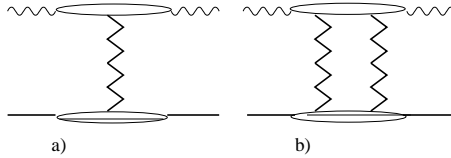


Figure 1: *Photon-proton scattering via pomeron exchange: a) one-pomeron exchange graph, b) two-pomeron exchange graph.*

total cross section reads $\sigma_{\text{tot}} = \sigma^{(1)} - \sigma^{(2)}$, where $\sigma^{(1)}$ and $\sigma^{(2)}$ are the cross sections of the one- and two-pomeron exchange graphs, respectively. In RFT, the energy-dependence of the cross sections $\sigma^{(1)}$ and $\sigma^{(2)}$ can be estimated with $\sigma^{(1)} \sim s^{\Delta_B}$ and $\sigma^{(2)} \sim s^{2\Delta_B}$, $1 + \Delta_B$ being the bare pomeron intercept.

To link particle production to elastic scattering amplitudes, we use the optical theorem together with the AGK cutting rules⁴. Up to trivial kinematical factors, the discontinuity of elastic amplitude is equal to the squared matrix element describing particle production. In the framework of unitarity cuts, the discontinuity corresponds to an unitarity cut moving the particles of all crossed propagators on mass shell, e.g. all cut propagator lines become final state particles. For example, let's consider the total discontinuity of the two-pomeron graph. According to the AGK cutting rules, three different cut configurations are giving the dominant contributions: the diffractive cut with the weight -1 (Fig. 2 a)), the one-pomeron cut with the weight 4 (Fig. 2 b)), and the two-pomeron cut with the weight -2 (Fig. 2 c)). The cross sections for

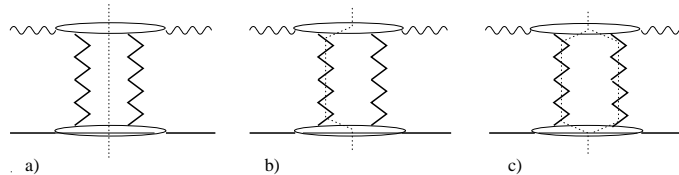


Figure 2: *Breakdown of the total discontinuity of the two-pomeron exchange graph according to the AGK cutting rules: a) the diffractive cut describing low-mass diffraction, b) the one-pomeron cut, and c) the two-pomeron cut.*

the different final states of the two-pomeron exchange graph are (i) diffractive cut: $\sigma_{\text{diff}} = \sigma^{(2)}$, (ii) one-pomeron cut: $\sigma_1 = -4\sigma^{(2)}$, and (iii) two-pomeron cut: $\sigma_2 = 2\sigma^{(2)}$. Note that the diffractive cut of the two-pomeron graph gets a negative AGK weight, hence giving in total a positive, experimentally observable cross section. However, the cross section for the one-pomeron cut of the two-pomeron graph is negative. Since the one-pomeron cut of the one-

pomeron graph has the same inelastic final state as the one-pomeron cut of the two-pomeron graph, one has to sum both contributions giving together a positive cross section.

2 Multiparticle production

Concerning the topologies of the final state particles, the total cross section is built up by the sum of the partial cross sections of the one- and two-pomeron exchange graphs: (i) one-pomeron cut (Fig.3 a)) $\sigma_1 = \sigma^{(1)} - 4 \sigma^{(2)}$,

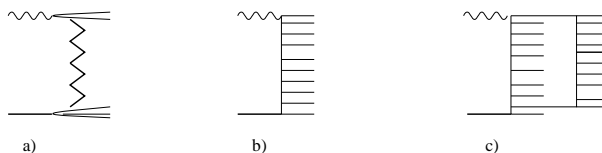


Figure 3: *Inelastic final states resulting from a) the diffractive cut describing low-mass diffraction, b) the one-pomeron cut, and c) the two-pomeron cut.*

(ii) two-pomeron cut (Fig.3 b)) $\sigma_2 = 2 \sigma^{(2)}$, and (iii) diffractive cut of the two-pomeron graph (Fig.3 c)) $\sigma_{\text{diff}} = \sigma^{(2)}$.

Let's consider a few applications of the AGK cutting rules to soft multiparticle production. The particle density in pseudorapidity of produced by a one-pomeron cut is assumed to be almost energy independent (which is true for longitudinal phase space models) and is denoted by $dN_1/d\eta$. Assuming that a two-pomeron cut gives two times the particle yield compared to the one-pomeron cut (in central pseudorapidity region, see Fig. 3), the inclusive inelastic charged particle cross section reads

$$\left. \frac{d\sigma_{\text{ch}}}{d\eta} \right|_{\eta \approx 0} = 1 \times \sigma_1 \frac{dN_1}{d\eta} + 2 \times \sigma_2 \frac{dN_1}{d\eta} + 0 \times \sigma_{\text{diff}} \frac{dN_1}{d\eta} = \sigma^{(1)} \frac{dN_1}{d\eta} \quad (2)$$

Due to the topology of diffractive final states, almost no particles are produced in the central region in the case of a diffractive cut. Note that only the one-pomeron graph determines the inclusive particle cross section in the central region (AGK cancellation). Then, the inclusive charged particle pseudorapidity density reads

$$\left. \frac{dn_{\text{ch}}}{d\eta} \right|_{\eta \approx 0} = \frac{\sigma^{(1)}}{\sigma_{\text{tot}}} \left. \frac{dN_1}{d\eta} \right|_{\eta \approx 0} \approx \frac{\sigma^{(1)}}{\sigma^{(1)} - \sigma^{(2)}} \left. \frac{dN_1}{d\eta} \right|_{\eta \approx 0} \quad (3)$$

Eq. (3) allows to understand the observed behaviour of $\rho(0) = dn_{\text{ch}}/d\eta$ in pp and $p\bar{p}$ collisions. With $\sigma^{(1)} \sim s^{\Delta_B}$ and $\sigma_{\text{tot}} \sim s^{0.08}$, one get a power-

law increase of the central particle density. This is confirmed by experiment⁵: $\rho(0) \approx 0.74 s^{0.105}$. Since the two-pomeron graph has a cross section which increases faster with the energy than the cross section of one-pomeron graph, the model predicts also an increase of the multiplicity fluctuations with increasing collision energies. An consequence is the violation of KNO scaling^{6,7} at high energies. For example, model predictions for the multiplicity distribution and the pseudorapidity distribution (calculated with the PHOJET event generator^{8,9}) are compared with data^{10,11,5,12} in Fig. 4. Furthermore, due to

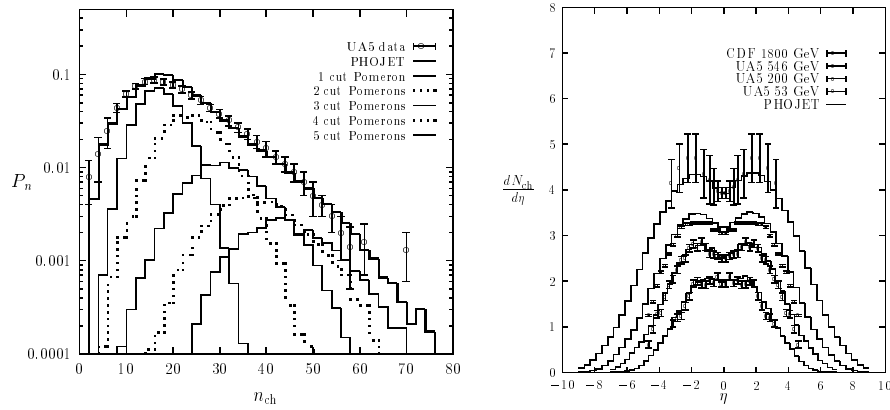


Figure 4: a) Decomposition of the multiplicity distribution in $p\bar{p}$ collisions according to the number of generated pomeron cuts at $\sqrt{s} = 200$ GeV. b) Increase of the charged particle pseudorapidity density in $p\bar{p}$ collisions with the energy.

the characteristic structure of the one- and two-pomeron cut, strong long-range correlations in pseudorapidity are naturally explained. For a detailed discussion, see for example¹³.

3 Application to photon-hadron scattering

All the important successes of the RFT and AGK based phenomenology encourage to apply this concept to photoproduction and the transition to DIS. From $x \approx Q^2/(s_{\gamma^*p} + Q^2)$ follows that low $x = 10^{-3} \dots 10^{-4}$ and medium $Q^2 = 5 \dots 30$ GeV² correspond to the Regge limit of γ^*p scattering.

There are two important new effects to note: **(i)** the photon has a dual nature and can interact as a gauge boson (pointlike) or a hadron (resolved), and **(ii)** the photon has an additional degree of freedom, the photon virtuality. Both effects give a handle to suppress the relative size of the unitarity

corrections (e.g. the relative size of the multi-pomeron graphs compared to the one-pomeron exchange). In direct photon interactions, there is no hadronic remnant to allow for multiple interactions (e.g. two-pomeron exchange). Considering γ^*p scattering with not too small Q^2 , the cross sections $\sigma^{(n)}$, ($n \geq 2$) are suppressed at least by a factor $1/Q^2$ compared to $\sigma^{(1)}$. Hence, multiple interaction contributions decrease with increasing Q^2 . Furthermore, resolved photon interactions are more suppressed with increasing Q^2 than direct photon interactions.

Concerning photoproduction, multiple interaction models predict a larger transverse energy deposit in resolved photon interactions than in direct photon interactions. In jet production via resolved photon collisions, additional interactions produce the so-called jet pedestal effect (which is absent in direct photon interactions). Recently, this has been confirmed in jet measurements at HERA^{14,15,16}.

The same arguments can be applied to photon diffraction dissociation in photoproduction. In RFT inspired models, the diffractive cross section would grow with the energy like $\sigma_{\text{diff}} \sim (s_{\gamma^*p})^{2\Delta_B}$. The measured flat energy dependence is explained due to unitarity corrections: additional interactions produce particles filling the rapidity gap of the diffractive interaction. This can be parametrized effectively introducing a *rapidity gap survival probability*⁷. The important point is that the rapidity gap survival probability in hard diffraction differs significantly between direct and resolved photon interactions. Rapidity gap events with a resolved hard photon interaction are suppressed by a factor of about 2...3 compared to events with direct hard photon interactions. Knowing the diffractive proton structure function (from DIS measurements, gluon densities determined from scaling violation), this effect can be measured easily and allows to check the concept of the rapidity gap survival probability.

For DIS, the limit $\sigma_{\text{tot}} \gg \sigma_{\text{diff}}$ can be satisfied by selecting events with not too small Q^2 . Then, AGK cancellation would predict for different Q^2 and x , (using $\sigma_{\text{diff}} = \sigma^{(2)}$, see Eq. (3))

$$\left(\frac{\sigma_{\text{tot}}}{\sigma_{\text{tot}} + \sigma_{\text{diff}}} \right) \frac{dn_{\text{ch}}}{d\eta} \bigg|_{\eta \approx 0} \approx \text{const}, \quad (4)$$

where the charged particle density is always normalized to the total cross section. Note that the diffractive cross section σ_{diff} is the cross section of quasi-elastic vector meson production and diffraction dissociation. Furthermore, in this limit, the energy-dependence of the cross section for quasi-elastic ρ^0 production σ_{ρ^0} is almost the same as the energy-dependence of $\sigma^{(2)}$: $\sigma_{\rho^0} \sim \sigma^{(2)} \sim (s_{\gamma^*p})^{2\Delta_B}$.

Further predictions are straight forward: for example, with increasing photon virtuality,

- (i) the jet pedestal effect decreases for jets at central c.m. pseudorapidity
- (ii) multiplicity fluctuations decrease
- (iii) long-range multiplicity fluctuations decrease.

Eventually, it should be mentioned that the phenomenology using RFT and AGK cutting rules suffers corrections due to energy-momentum conservation effects. It is very difficult to estimate these corrections without a detailed Monte Carlo model study.

Acknowledgments

We acknowledge valuable discussions with A. Capella and A. Kaidalov. One of the authors (R.E.) was supported by the Deutsche Forschungsgemeinschaft under contract No. Schi 422/1-2.

References

1. V. N. Gribov: Zh. Eksp. Teor. Fiz. 26 (1968) 414
2. V. N. Gribov: Zh. Eksp. Teor. Fiz. 26 (1969) 1306
3. M. Baker and K. A. Ter-Martirosyan: Phys. Rep. 28C (1976) 1
4. V. A. Abramovski, V. N. Gribov and O. V. Kancheli: Sov. J. Nucl. Phys. 18 (1974) 308
5. UA5 Collab.: G. J. Alner et al.: Z. Phys. C33 (1986) 1
6. Z. Koba, H. Nielsen and P. Olesen: Nucl. Phys. B40 (1972) 317
7. Z. Koba, H. Nielsen and P. Olesen: Nucl. Phys. C29 (1972) 201
8. R. Engel: Z. Phys. C66 (1995) 203
9. R. Engel and J. Ranft: Phys. Rev. D54 (1996) 4244
10. UA5 Collab.: R. E. Ansorge et al.: Z. Phys. C43 (1989) 357
11. UA5 Collab.: K. Alpgard et al.: Phys. Lett. 112B (1982) 183
12. CDF Collab.: F. Abe et al.: Phys. Rev. D41 (1990) 2330
13. A. Capella, U. Sukhatme, C. I. Tan and J. Trân Thanh Vân: Phys. Rep. 236 (1994) 227
14. H1 Collab.: I. Abt et al.: Phys. Lett. B314 (1993) 436
15. H1 Collab.: S. Aid et al.: Z. Phys. C70 (1995) 17
16. ZEUS Collab.: M. Derrick et al.: Phys. Lett. B342 (1995) 417
17. J. D. Bjorken: Phys. Rev. D47 (1992) 101